

---

---

# A Multi-Body Dynamic Study on the Torsional Vibrations of a Propulsion Shaft System

Jing Liu, Chenyan Zhao, Yuchen An and Guang Pan

*School of Marine Science and Technology, Northwestern Polytechnical University, Xi'an, 710072, P. R. China.  
Laboratory for Unmanned Underwater Vehicle, Northwestern Polytechnical University, Xi'an, 710072, P. R. China. E-mail: jliu@cqu.edu.cn*

(Received 5 November 2024; accepted 14 April 2025)

The torsional vibrations of the propulsion shaft system in unmanned underwater vehicles (UUVs) could significantly affect the system's fatigue life and acoustic stealth performance. Therefore, it is important to study the torsional vibrations of the propulsion shaft system. This paper establishes a dynamic model of a propulsion shaft system in the unmanned vehicles. The model demonstrates the effects of the torsional stiffness of the shafts and the flexible coupling. The vibrations of the propulsion shaft system are calculated by a commercial software. The effects of the torsional stiffness of the flexible coupling and the rotational speed on the torsional vibrations are analyzed. This work could provide some theoretical foundation for the design and torsional vibration optimization of the propulsion shaft system in UUVs.

---

## 1. INTRODUCTION

The propulsion shaft system is the main source of vibration and noise in unmanned underwater vehicles (UUVs), which has a great influence on their fatigue life and reliability. The torsional vibrations of the propulsion shaft system can be effectively reduced by utilizing a flexible coupling with appropriate torsional stiffness, then the system's natural frequency would be also lowered. Furthermore, the free and forced vibrations of the system would be affected by the torsional stiffness of the shafts, which should be considered in the modeling process. It is essential to study and optimize the torsional vibrations of the propulsion shaft system in UUVs.

There have been many studies that demonstrate the dynamic modeling methods of the shaft-bearing systems (SBSs). Huang et al.<sup>1</sup> presented a dynamics model of a SBS based on the frequency response function-based substructuring (FBS) method that incorporates a real propeller. The results showed that the propeller flexibility should be considered for the vibro-acoustic analysis. Chu et al.<sup>2</sup> established a dynamic model of a shaft system based on the transfer matrix method. The shaft was defined as a series of continuous mass. The effects of rotational speeds and static thrusts on the longitudinal vibrations were investigated. Liew et al.<sup>3</sup> presented a nonlinear rotor bearing system by a transient solution technique. Its versatility was evaluated by analyzing the flexible SBS with the hydrodynamic and deep-groove ball bearings. Li et al.<sup>4</sup> established a dynamic model of a SBS with the load, elastic deformation and hydrodynamic film. The effects of the fan and pulley unbalances on the vibrations of the system were investigated. Huang et al.<sup>5</sup> presented a dynamic model of a SBS by using a round Euler-Bernoulli beam. The effect of a bearing type on the instability of a spindle system and rotational speed was studied. Arun et al.<sup>6</sup> established a dynamic model of the SBS based on the finite element (FE) rotor model. The accuracy of FE method for a simple SBS was demonstrated. Han and

Chu<sup>7</sup> presented a dynamic model of SBS based upon the energy theorem and Lagrange's principle. The effects of rolling motion, pitching and yawing motions and damping were studied. Mohammad et al.<sup>8</sup> established a high-speed rotor model by using the 3-dimensional finite element model (3D FEM) and 1D beam model. The results indicated that the 1D beam model could be used for rotor dynamic analysis with some acceptable accuracy. Brouwer et al.<sup>9</sup> established a flexible shaft model with a full 3D elastic formulation by using the explicit FE method. The simulation and the experimental results were similar. Thus, the flexible dynamic model is more accurate by considering the deformation of the shafts. The calculation efficiency of modal superposition is high since the influence of high-frequency modes was ignored.<sup>10</sup> Therefore, the modal superposition method should be combined with the finite element method to obtain the ideal accuracy and efficiency.

The current torsional vibration analysis mainly studied the natural frequencies and the forced vibrations of the SBSs. Drab et al.<sup>11</sup> established a multi-body dynamics model of crankshaft by using the Buckens frame. The coupled vibration speed response laws at the resonance speed points and the vibration response law of the shaft system were studied. Some studies applied the FE method to investigate the natural frequencies of SBSs. Ma et al.<sup>12</sup> presented a multiple dynamics model of a SBS with the blade-tip rubbing by using the Timoshenko beam. The effects of rotational speed, stagger angle and casing stiffness were analyzed. Liu et al.<sup>13</sup> presented a dynamic model for a shaft system of reciprocating compressor based on the modal superposition method. The maximum torsional angle of the lumped-mass model of the SBS under a cyclic excitation load was analyzed. Huang et al.<sup>14</sup> presented a simplified lumped-mass model of a SBS and obtained the theoretical solution to validate the dynamic model. The effects of rotational speed and loading condition were investigated. The studies showed that the calculation model of torsional vibra-

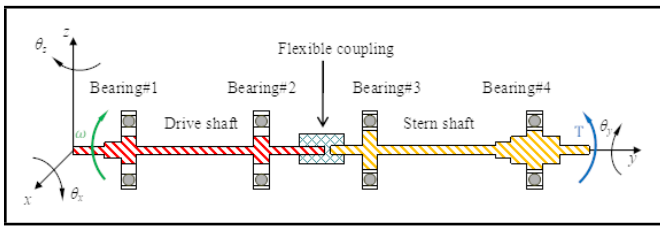


Figure 1. Schematic diagram of a flexible shaft system.

tions for SBSs could be classified as the lumped-mass model and the continuous distribution model. In the lumped-mass model method, the shaft system was discretized into a spring-mass model.<sup>15</sup> In the continuous model method, the mass of the shaft was distributed along the axis and the shape of the shaft was considered.<sup>11</sup> However, the calculation of the continuous model was complicated. For some studies, the natural frequencies were obtained by the FEM.<sup>16</sup> Huang et al.<sup>17</sup> established a coupled torsional-longitudinal vibration model of a drive shaft. The effects of the coupled vibrations caused by the variation of rotational speed and loading condition on the natural frequencies and maximum amplitudes were investigated. However, there are few studies for the effect of the torsional stiffness of flexible coupling on the propulsion shaft system.

This paper presents a flexible dynamic model of a propulsion shaft system in the UUV. The contact forces of the supporting bearings are calculated based on the Hertzian contact theory. The influences of geometrical parameters of bearings are considered. The dynamic responses of the propulsion shaft system are calculated by using the model superposition method, which considers the shaft torsional deformation. The influences of torsional stiffness and rotational speed on the characteristics of the torsional vibrations are studied.

## 2. DYNAMIC MODELLING OF A FLEXIBLE PROPULSION SHAFT SYSTEM

The schematic diagram of the propulsion shaft system is given in Fig. 1,  $\omega$  is the system rotational speed,  $T$  is the load torque. The propulsion shaft system consists of a drive shaft and a stern shaft. The stern shaft is connected to the drive shaft by a flexible coupling. The flexible coupling is simplified as a six-degrees of freedom (6-DOF) linear spring unit. The shell structure is treated as the rigid body. The motions of the shell structure are ignored. The drive shaft and stern shaft are modeled as the flexible parts. Then, the torsional stiffness of the shaft could be considered. The drive shaft and the stern shaft are installed on the shell structure by four supporting bearings. Furthermore, the effects of the mass and the moment of inertia of the motor and the propeller and the gravity of the shaft are ignored.

### 2.1. A Finite Element Calculation Model of the Propulsion Shaft System

A flexible dynamic model of the propulsion shaft system is established by using a commercial software as shown in Fig. 2. The inner ring of the supporting bearing is connected to the flexible shaft, the outer ring is rigidly fixed to the shell structure. The speed boundary condition is applied to the drive shaft

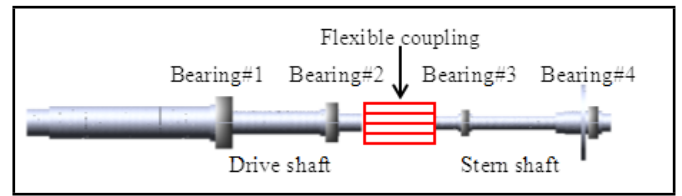


Figure 2. A calculation model of the flexible propulsion shaft system.

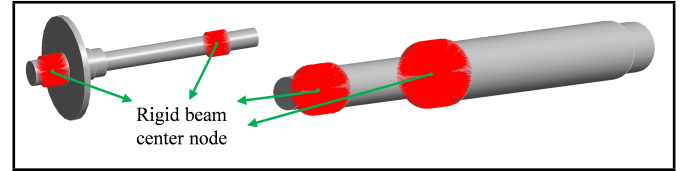


Figure 3. The rigid region of the flexible shaft.

at the location of bearing #1. The torque load is applied at the end of the stern shaft. The 3D finite element models of the drive shaft and stern shaft are established for the calculation model. The finite element size of the flexible shaft is 3 mm. The drive shaft has 453777 elements and 106496 nodes. The stern shaft has 132482 elements and 29004 nodes.

The master nodes and slave nodes should be introduced for the force transmission process in the commercial software. The rigid region is established to simplify the calculation model and facilitate load transfer as given in Fig. 3. The rigid regions could be obtained around the master and slave nodes. The master node coincides with the geometric center of the shaft journal. The center node of the supporting bearings is designated as the master node. The nodes of the shaft connected to the bearings are designated as slave nodes. The master node is connected to the slave nodes using a rigid beam.

### 2.2. Dynamic Modeling of the Supporting Bearings

The rolling bearings are selected as the supporting bearings of the propulsion shaft system, which can be simplified as 2-DOF vibration system.<sup>20</sup> The dynamic modeling of the rolling bearing is given in Fig. 3. The equations of the rolling bearing are:

$$\begin{cases} m\ddot{x} + c\dot{x} + F_x = Q_x \\ m\ddot{y} + c\dot{y} + F_y = Q_y \end{cases}; \quad (1)$$

where  $m$  is the mass of the shaft and the inner ring of the rolling bearing,  $c$  is the damping coefficient of the propulsion shaft system,  $Q_x$  and  $Q_y$  are the loads in x axis and y axis directions, respectively.  $F_x$  and  $F_y$  are the contact forces in x axis and y axis directions, respectively, which is given by:

$$\begin{cases} F_x = K_T \sum_i^N \beta_i \delta_i^n \cos \theta_i \\ F_y = K_T \sum_i^N \beta_i \delta_i^n \sin \theta_i \end{cases}; \quad (2)$$

where  $K_T$  is the contact stiffness of the bearing,  $N$  is the ball number,  $\delta_i^n$  is the total deformation among the  $i$ -th ball, bearing inner and outer raceway,  $\theta_i$  is the angle displacement of the ball,  $\beta_i$  is a parameter for determining the occurrence of

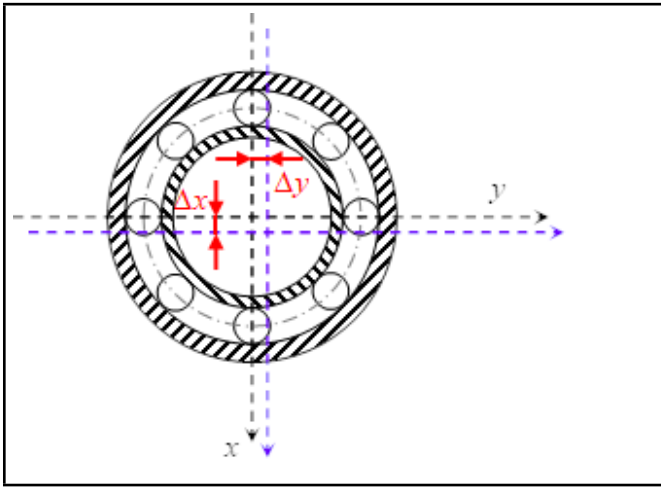


Figure 4. Dynamic modelling of the supporting bearings.

contact deformation, which is given by:

$$\beta_i = \begin{cases} 1, \delta_i > 0 \\ 0, \delta_i < 0 \end{cases} \quad (3)$$

### 2.3. Dynamic Modeling of the Flexible Coupling

The flexible coupling could be simplified as a 6-DOF linear spring unit, the stiffness and damping matrices are given by:

$$K_c = \text{diag}(k_x \quad k_y \quad k_z \quad k_{\theta_x} \quad k_{\theta_y} \quad k_{\theta_z}); \quad (4)$$

$$C_c = \text{diag}(c_x \quad c_y \quad c_z \quad c_{\theta_x} \quad c_{\theta_y} \quad c_{\theta_z}); \quad (5)$$

where  $k_x, k_y, k_z$  and  $k_{\theta_x}, k_{\theta_y}, k_{\theta_z}$  are the stiffness in  $x, y, z$  and  $\theta_x, \theta_y, \theta_z$  directions;  $c_x, c_y, c_z$  and  $c_{\theta_x}, c_{\theta_y}, c_{\theta_z}$  are the damping coefficient in  $x, y, z$  and  $\theta_x, \theta_y, \theta_z$  directions.  $k_x$  and  $k_y$  are the stiffness coefficient in radial direction, so  $k_x = k_y$ . Similarly,  $c_{\theta_x} = c_{\theta_y}$ .

Then, the force caused by the flexible coupling is:

$$F_c = K_c(u_m - u_s) + C_c(\dot{u}_m - \dot{u}_s); \quad (6)$$

where  $u_m$  and  $u_s$  are the displacements of the drive shaft and the stern shaft, respectively.  $\dot{u}_m$  and  $\dot{u}_s$  are the velocities of the drive shaft and the stern shaft, respectively.

### 2.4. Dynamic Modeling of the Flexible Shaft

The dynamic model and the corresponding coordinate of the flexible shaft are given in Fig. 5. The position vector  $r_p$  of any point  $P$  on the flexible shaft relative to the inertial coordinate system is given by:

$$r_p = r_{o'} + Au; \quad (7)$$

where  $r_{o'}$  is the position vector of the floating coordinate system relative to the inertial coordinate system,  $A$  is the transformation matrix from the floating coordinate system to the inertial coordinate system, and  $u$  represents the position of point  $P$  in the floating coordinate system.

The flexible body is discretized by using the Rayleigh-Ritz method, which is:

$$u_f = \Phi q_f; \quad (8)$$

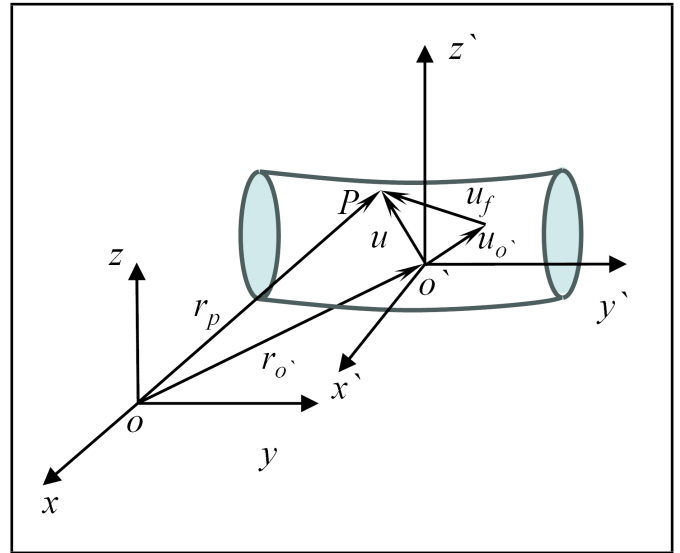


Figure 5. Schematic of a flexible shaft.

where  $u_f$  is the relative position vector of point  $P$  after deformation relative to its position before deformation;  $\Phi$  is the shape function deformation mode matrix and  $q_f$  is the deformation generalized matrix. The speed vector at point  $P$  is given by:

$$\dot{r}_p = \dot{r}_{o'} + \dot{A}u_{o'} + A\Phi\dot{q}_f; \quad (9)$$

where  $u_{o'}$  is the relative position vector before the deformation at point  $P$ .

The dynamic equations for each part of the propulsion shaft system can be assembled into corresponding matrices, along with the relevant constraint equations. This results in the dynamical control equations for the flexible propulsion shaft system are:

$$\begin{cases} Q_F = M\ddot{q} + \dot{M}\dot{q} - \frac{1}{2} \left[ \frac{\partial M}{\partial \dot{q}} \dot{q} \right]^T + Kq + Z\dot{q} + \left[ \frac{\partial C}{\partial q} \right]^T \lambda \\ C(q, t) = 0 \end{cases}; \quad (10)$$

where  $Q_F$  is the generalized force matrix,  $M$  is the mass matrix,  $K$  is the generalized stiffness matrix for flexible generalized coordinates,  $Z$  is the damping matrix of the flexible body,  $C_q^i$  represents the constraint equations, and denotes the Lagrange multipliers.

## 3. RESULTS AND DISCUSSIONS

The parameters of the four supporting bearings in Fig. 1 are shown in Table 1. The torsional stiffness of the flexible coupling is taken as  $k = 300 \text{ Nm}^\circ, k = 400 \text{ Nm}^\circ, k = 500 \text{ Nm}^\circ, k = 600 \text{ Nm}^\circ, k = 700 \text{ Nm}^\circ, k = 800 \text{ Nm}^\circ, k = 900 \text{ Nm}^\circ$  and  $k = 1000 \text{ Nm}^\circ$ . The simulation step size is set to 0.0001 seconds, with a simulation duration of 0.2 seconds for the free vibrations and 5 seconds for the forced vibrations.

## 4. THE EFFECT OF TORSIONAL STIFFNESS ON THE FORCED VIBRATIONS

The impact method is used for free torsional vibration analysis in this study.<sup>18</sup> An impulse is applied to the propulsion shaft

**Table 1.** Parameters of the supporting bearings.

Bearings	Parameters	Values	Unit
#1	Pitch diameter	102.500	Mm
	Ball number	18	—
	Ball diameter	10.319	mm
	Inner raceway radius in radial section	5.260	mm
	Outer raceway radius in radial section	5.370	mm
	Radial clearance	C0	—
#2	Pitch diameter	69.014	mm
	Ball number	20	—
	Ball diameter	5.820	mm
	Inner raceway radius in radial section	3.026	mm
	Outer raceway radius in radial section	3.085	mm
	Radial clearance	C0	—
#3	Pitch diameter	51.510	mm
	Ball number	20	—
	Ball diameter	4.236	mm
	Inner raceway radius in radial section	2.203	mm
	Outer raceway radius in radial section	2.245	mm
	Radial clearance	C0	—
#4	Pitch diameter	57.511	mm
	Ball number	22	—
	Ball diameter	4.253	mm
	Inner raceway radius in radial section	2.211	mm
	Outer raceway radius in radial section	2.254	mm
	Radial clearance	C0	—

**Table 2.** Effect of torsional stiffness on the natural frequencies.

Torsional stiffness/(Nm/°)	Natural frequency/(Hz)
300	335
400	385
500	430
600	470
700	503
800	537
900	568
1000	594

system. Then, the free torsional vibrations are analyzed. The natural frequencies of the propulsion shaft system under different torsional stiffness values are calculated, as shown in Fig. 6. The free vibration exhibits a distinct characteristic frequency that increases when the flexible coupling stiffness increases, which is given in Table 2. The natural frequencies of the torsional vibration system rise from 335 Hz to 594 Hz when the torsional stiffness  $k$  is from 300 Nm/° to 1000 Nm/°. The amplitude of the free vibration waveform decreases due to the internal structural damping. The amplitude of the free vibration waveform increases with the rise of stiffness. Therefore, the system natural frequencies can be reduced by reducing the torsional stiffness of the flexible coupling, which is beneficial for optimizing the vibrations of the shaft system.<sup>19</sup> The torsional stiffness of the flexible couplings is taken as  $k = 300 \text{ Nm/}^\circ$ ,  $k = 400 \text{ Nm/}^\circ$ ,  $k = 500 \text{ Nm/}^\circ$ ,  $k = 600 \text{ Nm/}^\circ$ ,  $k = 700 \text{ Nm/}^\circ$ ,  $k = 800 \text{ Nm/}^\circ$ ,  $k = 900 \text{ Nm/}^\circ$  and  $k = 1000 \text{ Nm/}^\circ$ . The rotational speed of the propulsion shaft system is taken as 12000 r/min.

The effect of torsional stiffness on the forced vibrations is analyzed, which is given in Fig. 7, the steady-state response of forced vibrations exhibits a singular characteristic frequency, which corresponds to the excitation frequency. When the torsional stiffness values increase from 200 Nm/° to 300 Nm/°, the amplitude of the forced vibration waveform increases with

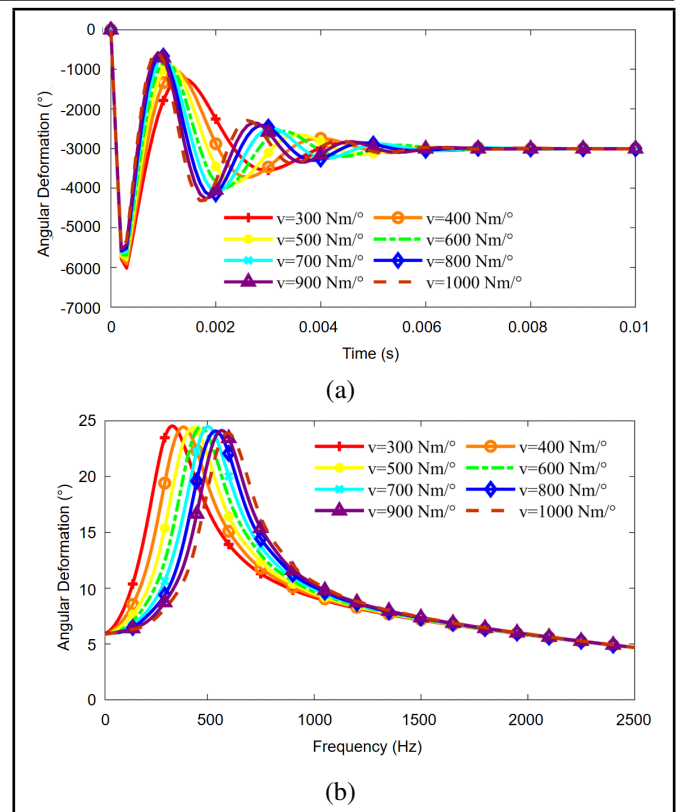


**Figure 6.** Effect of torsional stiffness on the free vibrations (a) time domain waveform and (b) spectra.

the increment of torsional stiffness. When the torsional stiffness values increase from 300 Nm/° to 1000 Nm/°, the amplitude of the forced vibration waveform decreases with the increment of torsional stiffness. The root mean square (RMS), Peak-to-Peak Value (PPV), and Fundamental Frequency Amplitude (FFA) values of the system under different torsional stiffnesses are given in Fig. 8. When the torsional stiffness increases from 200 Nm/° to 300 Nm/°, the RMS, PPV and FFA values increase with the increment of torsional stiffness. When the torsional stiffness is 300 Nm/°, the RMS value is 0.00233 °, the PPV value is 0.00660 °, and the FFA value is 0.00329 °. When the torsional stiffness increases from 300 Nm/° to 1000 Nm/°, the RMS, PPV, and FFA values decrease with the torsional stiffness increasing. Specifically, when the torsional stiffness is 1000 Nm/°, the RMS value is 0.00169 °, the PPV value is 0.00480 °, and the FFA value is 0.00239 °.

#### 4.1. The Effect of Rotational Speed on the Forced Vibration

The rotational speed of the propulsion shaft system is taken as 12000 r/min, 18000 r/min, 24000 r/min, 30000 r/min, 36000 r/min, 42000 r/min, 48000 r/min, 54000 r/min and 60000 r/min. The torsional stiffness of the flexible coupling is taken as 1000 Nm/°.

The effect of rotational speed on the forced vibrations is analyzed, which is given in Fig. 9, the steady-state response of forced vibrations exhibits a singular characteristic frequency, which corresponds to the excitation frequency. When the rotational speed values increase from 12000 r/min to 24000 r/min,

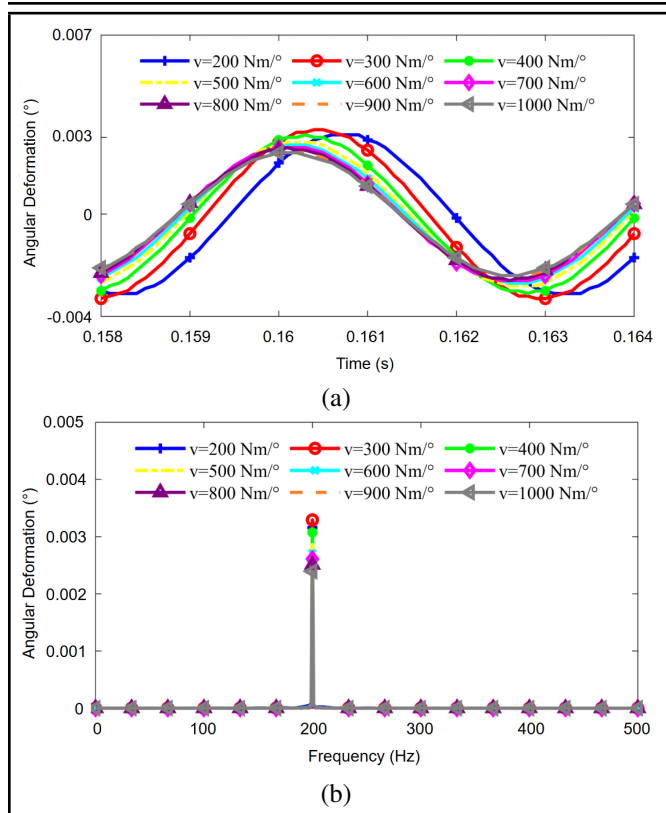


Figure 7. Effect of torsional stiffness on the forced vibrations (a) time domain waveform and (b) spectra.

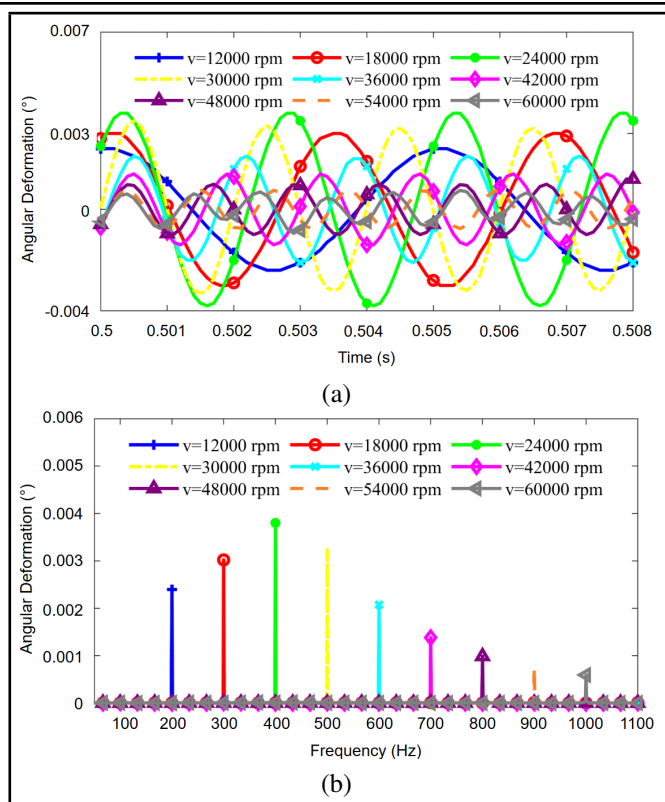


Figure 9. Effect of rotational speed on the forced vibration (a) time domain waveform and (b) spectra.

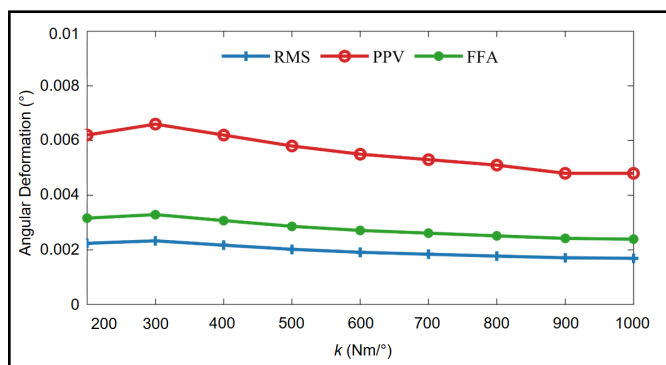


Figure 8. Effect of torsional stiffness on the RMS, PPV and FFA values.

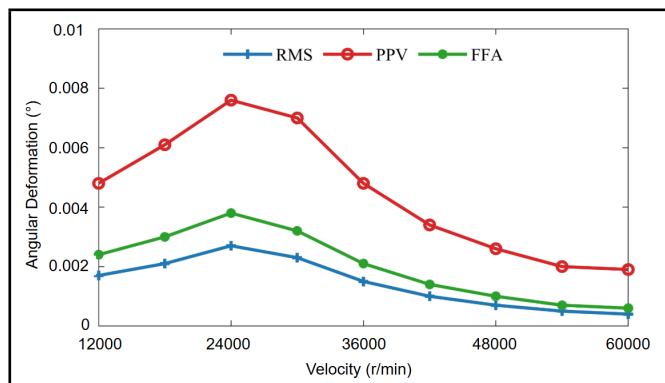


Figure 10. Effect of rotational speed on the RMS, PPV and FFA values.

the amplitude of the forced vibration waveform increases with the increment of rotational speed. When the rotational speed values increase from 24000 r/min to 60000 r/min, the amplitude of the forced vibration waveform decreases with the increment of rotational speed. The RMS, PPV and FFA values of the system under different rotational speed are given in Fig. 10. When the rotational speed increases from 12000 r/min to 24000 r/min, the RMS, PPV and FFA values increase with the increment of rotational speed. When the rotational speed is 24000 r/min, the RMS value is 0.00269 °, the PPV value is 0.00760 °, and the FFA value is 0.00380 °. When the rotational speed increases from 24000 r/min to 60000 r/min, the RMS, PPV and FFA values decrease with the increment of rotational speed. Specifically, when the rotational speed is 60000 r/min, the RMS value is 0.00044 °, the PPV value is 0.00197 °, and the FFA value is 0.00059 °.

### 5. THE COUPLED EFFECTS OF TORSIONAL STIFFNESS AND ROTATIONAL SPEED ON THE FORCED VIBRATION

The torsional stiffness of the flexible couplings is taken as  $k = 300 \text{ Nm/}^\circ$ ,  $k = 400 \text{ Nm/}^\circ$ ,  $k = 500 \text{ Nm/}^\circ$ ,  $k = 600 \text{ Nm/}^\circ$ ,  $k = 700 \text{ Nm/}^\circ$ ,  $k = 800 \text{ Nm/}^\circ$ ,  $k = 900 \text{ Nm/}^\circ$  and  $k = 1000 \text{ Nm/}^\circ$ . The rotational speed of the propulsion shaft system is taken as 12000 r/min, 18000 r/min, 24000 r/min, 30000 r/min, 36000 r/min, 42000 r/min, 48000 r/min, 54000 r/min and 60000 r/min. The coupled effects of torsional stiffness and speed on the forced vibration is analyzed.

In Fig. 11, when the torsional stiffness is 200  $\text{Nm/}^\circ$ , the RMS, PPV and FFA values reach the maximum at the rotational speed of 12000 r/min. The maximum values of the RMS, PPV and FFA are 0.00224 °, 0.00720 °, 0.00316 ° separately. When the torsional stiffness is 400  $\text{Nm/}^\circ$ , the RMS,

PPV and FFA values reach the maximum at the rotational speed of 18000 r/min. The maximum values of the RMS, PPV and FFA are  $0.00240^\circ$ ,  $0.00680^\circ$ ,  $0.00339^\circ$  separately. When the torsional stiffness is  $600 \text{ Nm}^\circ$ , the RMS, PPV and FFA values reach the maximum at the rotational speed of 18000 r/min. The maximum values of the RMS, PPV and FFA are  $0.00259^\circ$ ,  $0.00740^\circ$ ,  $0.00366^\circ$  separately. When the torsional stiffness is  $800 \text{ Nm}^\circ$ , the RMS, PPV and FFA values reach the maximum at the rotational speed of 24000 r/min. The maximum values of the RMS, PPV and FFA are  $0.00266^\circ$ ,  $0.00750^\circ$ ,  $0.00367^\circ$  separately. When the torsional stiffness is  $1000 \text{ Nm}^\circ$ , the RMS, PPV and FFA values reach the maximum at the rotational speed of 24000 r/min. The maximum values of the RMS, PPV and FFA are  $0.00269^\circ$ ,  $0.00760^\circ$ ,  $0.00380^\circ$  separately. When the rotational speed is 12000 r/min, the torsional vibrations of the propulsion shaft system reduce with the increment of torsional stiffness from  $200 \text{ Nm}^\circ$  to  $1000 \text{ Nm}^\circ$ ; when the rotational speed is 18000 r/min, the torsional vibrations of the propulsion shaft system increase with the increment of torsional stiffness from  $200 \text{ Nm}^\circ$  to  $600 \text{ Nm}^\circ$ , and reduce with the increment of torsional stiffness from  $600 \text{ Nm}^\circ$  to  $1000 \text{ Nm}^\circ$ ; when the rotational speed increases from 24000 r/min to 60000 r/min, the torsional vibrations of the propulsion shaft system increase with the increment of torsional stiffness from  $200 \text{ Nm}^\circ$  to  $1000 \text{ Nm}^\circ$ . The rotational speed at which the maximum values of the RMS, PPV and FFA occur increases with the increment of torsional stiffness.

## 6. CONCLUSIONS

This paper establishes a dynamic model of the propulsion system, considering the effect of torsional stiffness of the shaft. The effects of the torsional stiffness of the flexible coupling and the rotational speed were analyzed. The conclusions are listed below.

1. The natural frequencies of the propulsion shaft system could be reduced with the decrement of torsional stiffness of the flexible coupling. The natural frequencies of the propulsion shaft system increased from 335 Hz to 594 Hz when the torsional stiffness of the flexible coupling was from  $300 \text{ Nm}^\circ$  to  $1000 \text{ Nm}^\circ$ .
2. At a specific rotational speed, the torsional vibrations exhibited a nonlinear relationship with the torsional stiffness of the flexible coupling. When the rotational speed was 12000 r/min, the torsional vibrations of the propulsion shaft system rose when the torsional stiffness was from  $200 \text{ Nm}^\circ$  to  $300 \text{ Nm}^\circ$ ; and it decreased when the torsional stiffness was from  $300 \text{ Nm}^\circ$  to  $1000 \text{ Nm}^\circ$ .
3. At a specific torsional stiffness of the flexible coupling, the torsional vibrations exhibited a nonlinear relationship with the rotational speed. When the torsional was  $1000 \text{ Nm}^\circ$ , the torsional vibrations of the propulsion shaft system rose when the rotational speed was from 12000 r/min to 24000 r/min; and it decreased when the rotational speed was from 24000 r/min to 60000 r/min.

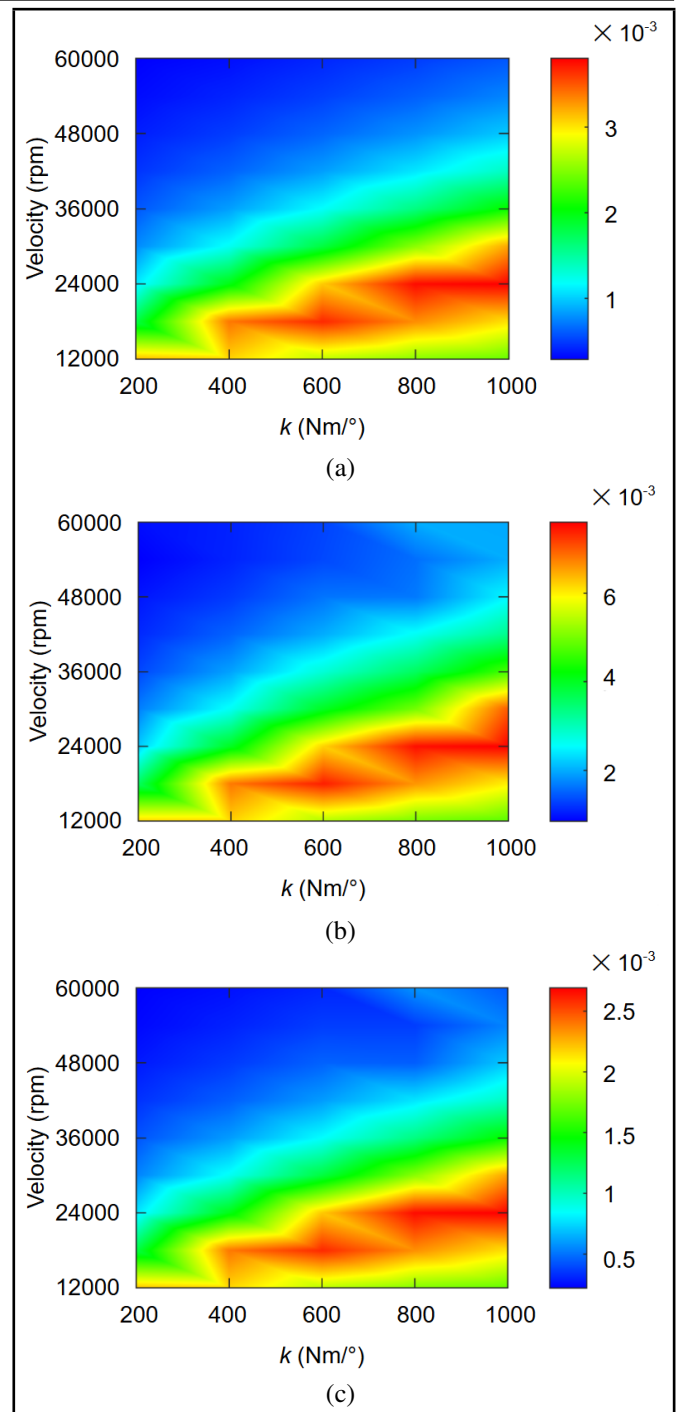


**Figure 11.** Effects of coupled torsional stiffness and speed on the (a) FFA values, (b) PPV values, and (c) RMS values.

4. The rotational speed at which the maximum values of the RMS, PPV and FFA occur increased with the increment of torsional stiffness.

## REFERENCES

- <sup>1</sup> Huang X.C., Ni Z. et al., Stiffness optimization of marine propulsion shafting system by FRF-based substructuring method and sensitivity analysis, *Ocean Engineering*, **144**, 243-256, (2017). <https://doi.org/10.1016/j.oceaneng.2017.08.042>
- <sup>2</sup> Chu W., Zhao Y. et al., Longitudinal vibration of ma-

- rine propulsion shafting: experiments and analysis, *Journal of Marine Science and Engineering*, **10**(9), 1173, (2022). <https://doi.org/10.3390/jmse10091173>
- <sup>3</sup> Liew A., Feng N.S., Hahn E.J., On using the transfer matrix formulation for transient analysis of non-linear rotor bearing systems, *International Journal of Rotating Machinery*, **10**(6), 425-431, (2004). <https://doi.org/10.1155/S1023621X04000429>
- <sup>4</sup> Li Z.M., Zhou Q., Tang J.P., An Q., Flexural vibration analysis of an automobile water pump bearing-rotor system with a modified transfer matrix method, *Journal of Multi-body Dynamics*, **226**(4), 331-342, (2012). <https://doi.org/10.1177/1464419312448300>
- <sup>5</sup> Bachschmid N., Pennacchi P., Tanzi E., Some remarks on breathing mechanism, on non-linear effects and on slant and helicoidal cracks, *Mechanical Systems and Signal Processing*, **22**(4), 879-904, (2008). <https://doi.org/10.1016/j.ymsp.2007.11.007>
- <sup>6</sup> Jalan A.K., Mohanty A.R., Model based fault diagnosis of a rotor-bearing system for misalignment and unbalance under steady-state condition, *Journal of Sound and Vibration*, **327**(3-5), 604-622, (2009). <https://doi.org/10.1016/j.jsv.2009.07.014>
- <sup>7</sup> Han Q.K., Chu F.L., Parametric instability of flexible rotor-bearing system under time-periodic base angular motions, *Applied Mathematical Modelling*, **39**(15), 4511-4522, (2015). <https://doi.org/10.1016/j.apm.2014.10.064>
- <sup>8</sup> Jalali M.H., Ghayour M., Ziaei-Rad S., Shahriari B., Dynamic analysis of a high speed rotor-bearing system, *Measurement*, **53**, 1-9, (2014). <https://doi.org/10.1016/j.measurement.2014.03.010>
- <sup>9</sup> Brouwer M.D., Sadeghi F., Ashtekar A., Archer J., Lancaster C., Combined explicit finite and discrete element methods for rotor bearing dynamic modeling, *Tribology Transactions*, **58**(2), 300-315, (2015). <https://doi.org/10.1080/10402004.2014.968699>
- <sup>10</sup> Lin C.G., Zou M.S., Sima C., Qi L.B., Yu Y., Non-linear coupled dynamics of a flexible propeller-shaft system supported by water film bearings, *Journal of Vibration and Acoustics*, **142**(3), 031008, (2020). <https://doi.org/10.1115/1.4046125>
- <sup>11</sup> Drab C.B., Engl H.W., Haslinger J.R. et al., Dynamic simulation of crankshaft multibody systems, *Multibody System Dynamics*, **22**, 133-144, (2009). <https://doi.org/10.1007/s11044-009-9152-8>
- <sup>12</sup> Ma H., Lu Y., Wu Z.Y. et al., Vibration response analysis of a rotational shaft-disk-blade system with blade-tip rubbing, *International Journal of Mechanical Sciences*, **107**, 110-125, (2016). <https://doi.org/10.1016/j.ijmecsci.2015.12.026>
- <sup>13</sup> Liu J., Sun X.D., Zhang X., Hou X.B., Research on torsional vibration characteristics of reciprocating compressor shafting and dynamics modification, *Mechanics of Advanced Materials and Structures*, **27**(9), 687-696, (2020). <https://doi.org/10.1080/15376494.2018.1492759>
- <sup>14</sup> Huang Q.W., Yan X.P. et al., Numerical modeling and experimental analysis on coupled torsional-longitudinal vibrations of a ship's propeller shaft, *Ocean Engineering*, **136**, 272-282, (2017). <https://doi.org/10.1016/j.oceaneng.2017.03.017>
- <sup>15</sup> Xiao N.Q., Zhou R.P. et al., Study on Vibration of marine diesel-electric hybrid propulsion system, *Mathematical Problems in Engineering*, (2016). <https://doi.org/10.1155/2016/8130246>
- <sup>16</sup> [Anonim], Study on the coupled torsional, axial, and bending three-dimensional vibrations of internal combustion engine shafting based on exact dynamic stiffness matrix methods, *Master's Thesis, Dalian University of Technology, Dalian, China*, (2006).
- <sup>17</sup> Huang Q.W., Yan X.P., Wang Y.K. et al., Numerical modeling and experimental analysis on coupled torsional-longitudinal vibrations of a ship's propeller shaft, *Ocean Engineering*, **136**, 272-282, (2017). <https://doi.org/10.1016/j.oceaneng.2017.03.017>
- <sup>18</sup> Xing P.F., Lu L.X. et al., A multi-method approach to identify the natural frequency of ship propulsion shafting under the running condition, *Journal of Marine Science and Engineering*, **10**(10), 1432, (2022). <https://doi.org/10.3390/jmse10101432>
- <sup>19</sup> Weiwei L., Study on torsional vibration of bulldozer drive system by elastic coupling, *Master's Thesis, Shandong Agricultural University, China*, (2007).
- <sup>20</sup> An Y., Liu C. et al., Multibody dynamic study and optimization for a flexible support shaft system in unmanned underwater vehicle, *Journal of Multi-body Dynamics*, **238**(2), 238-249, (2024). <https://doi.org/10.1177/14644193241238082>